REMOTE SENSING IN FIFE AND BOREAS

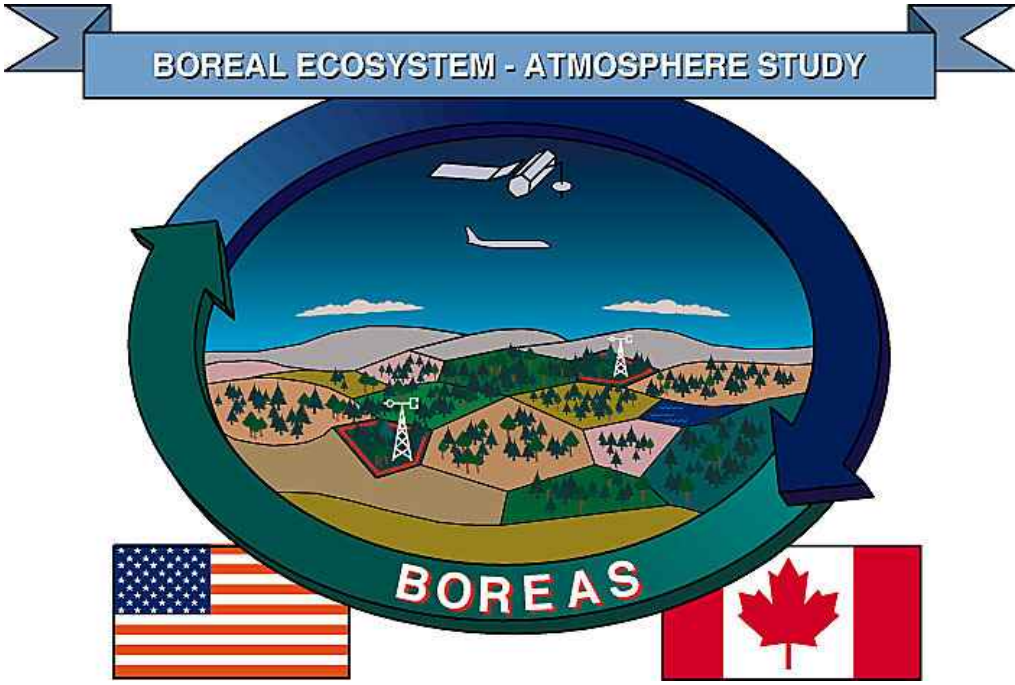

JOURNAL OF GEOPHYSICAL RESEARCH, VOL. 97, NO. D17, PAGES 18,345–18,371, NOVEMBER 30, 1992

An Overview of the First International Satellite Land Surface Climatology Project (ISLSCP) Field Experiment (FIFE)

P. J. SELLERS,[1] F. G. HALL,[1] G. ASRAR,[2] D. E. STREBEL,[3] AND R. E. MURPHY[2]

In the summer of 1983 a group of scientists working in the fields of meteorology, biology, and remote sensing met to discuss methods for modeling and observing land-surface–atmosphere interactions on regional and global scales. They concluded, first, that the existing climate models contained poor representations of the processes controlling the exchanges of energy, water, heat, and carbon between the land surface and the atmosphere and, second, that satellite remote sensing had been underutilized as a means of specifying global fields of the governing biophysical parameters. Accordingly, a multiscale, multidisciplinary experiment, FIFE, was initiated to address these two issues.

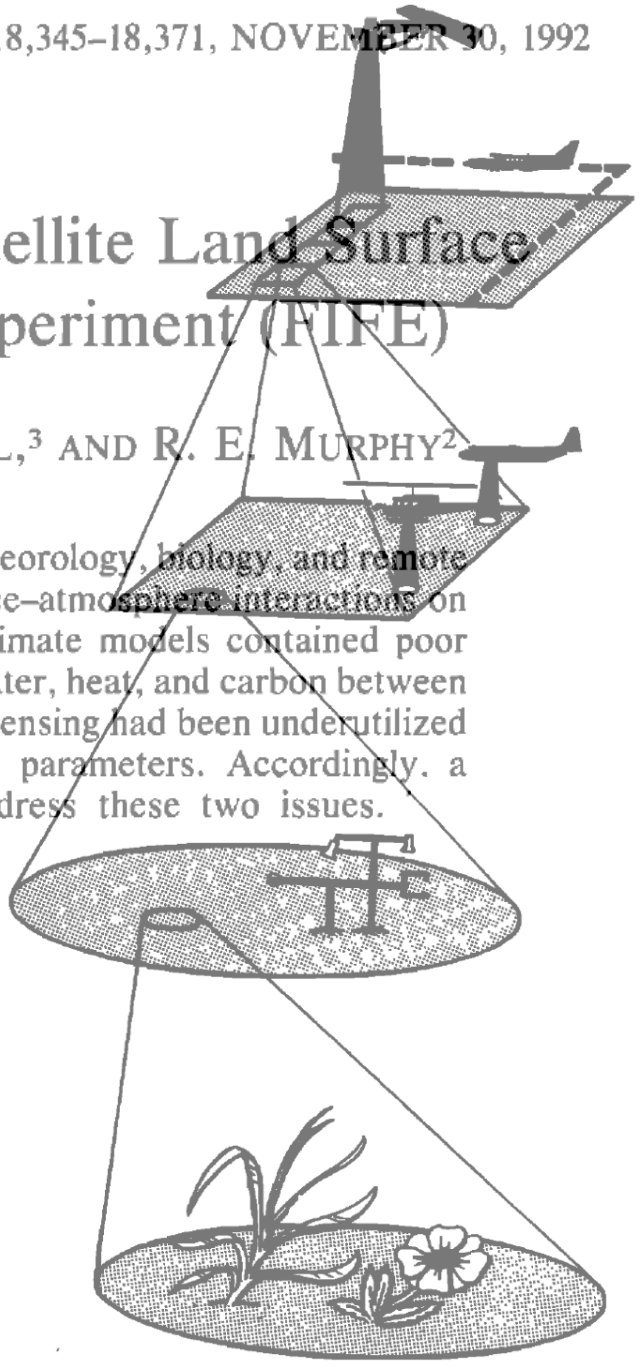

Fig. 1. Range of spatial scales addressed by FIFE.

Up and Down Scaling

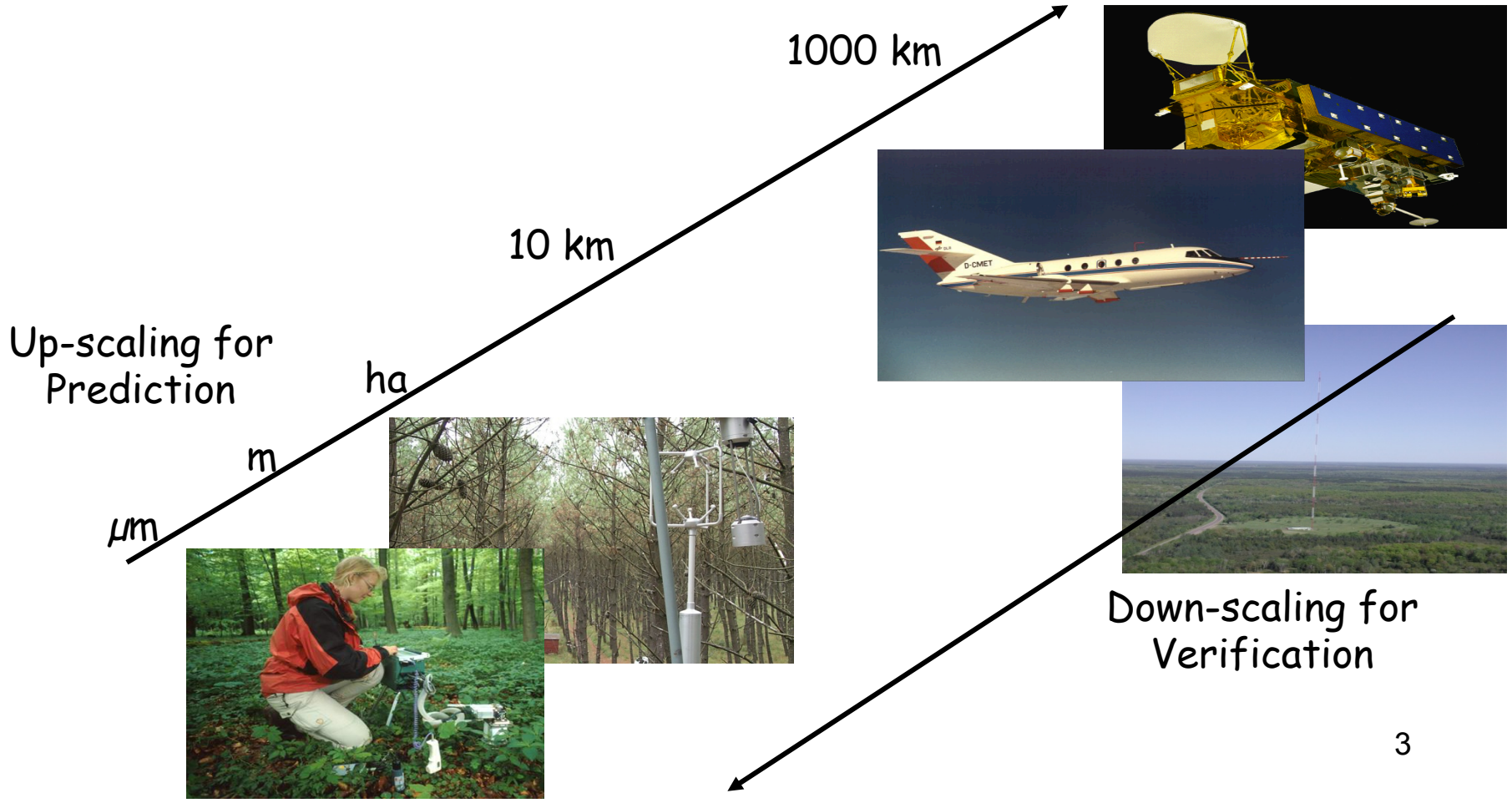

Surface Energy Budget

Net Radiation Absorbed = Net Short Wave {$Sw\downarrow(1-\alpha)$} + Net Long Wave {$Lw\downarrow - Lw\uparrow$}

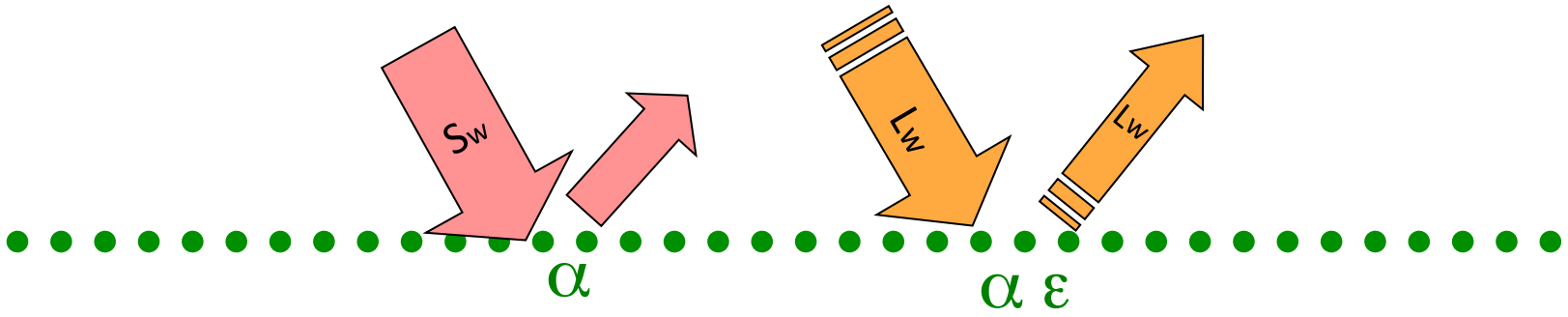

Remote Sensing Inputs

Atmospheric Aerosols and Clouds, Surface Albedo → Net Short Wave {Sw (1- ρ)}

Atmospheric
Water Vapor, Temperature Profiles, Cover Type (ε) → Net Long Wave {Lw ↓ Lw ↑}

Surface Heat and Mass Budget

R_n =Latent Heat (LE) + Sensible Heat (H) + Ground Heat Flux (G)

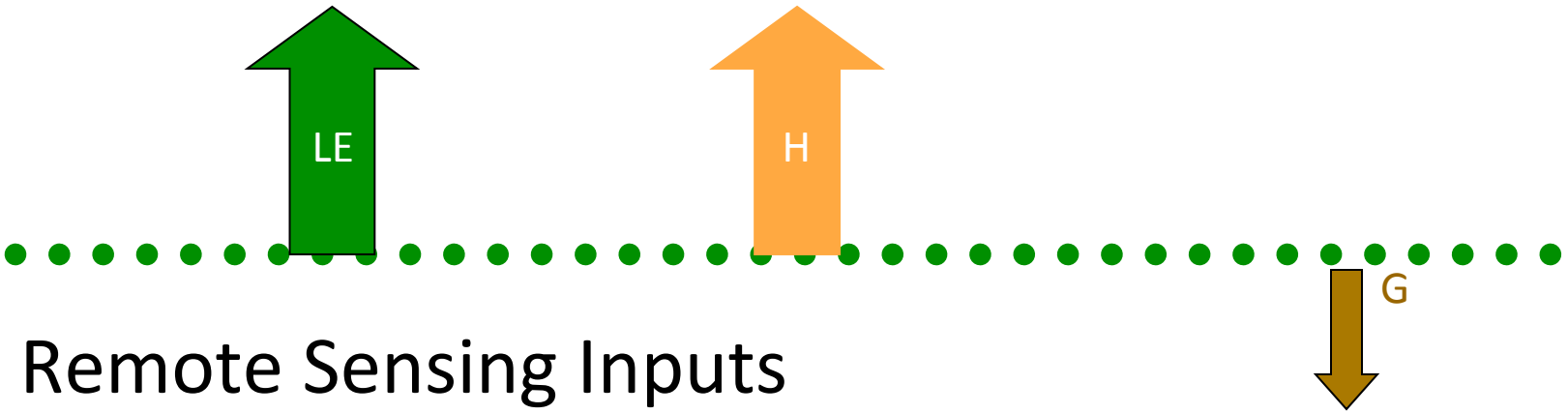

Remote Sensing Inputs

Fpar, Cover Type (C3 or C4), LAI → Latent Heat (LE)

Canopy Temperature, Air Temperature, Roughness Length, → Sensible Heat (H)

Snow Cover, Soil Moisture Content and State → Ground Heat Flux (G)

Surface Carbon Budget

Net Ecosystem Exchange = NEE

NEE=Gross Primary Production(GPP) - Autotrophic Respiration(R_a) - Heterotrophic Respiration(R_h)

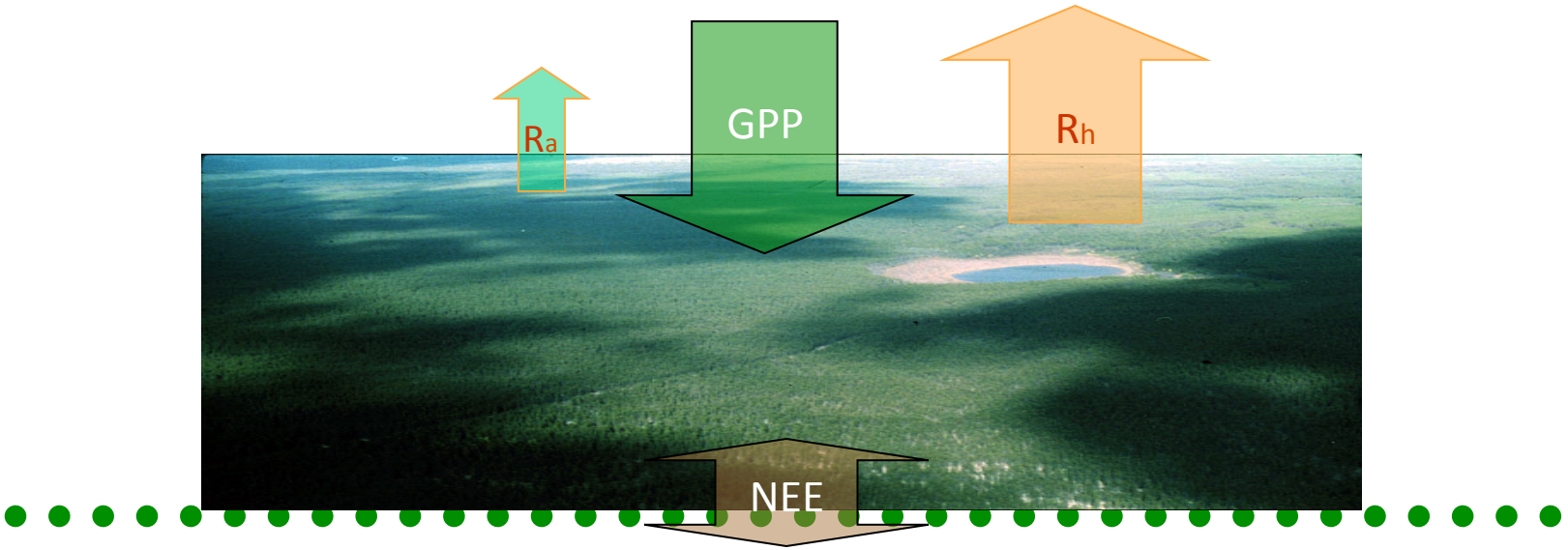

Remote Sensing Inputs

LAI, Fpar, Cover Type, Soil Moisture, Temperature → Gross Primary Production (GPP)

Biomass, Cover Type, Temperature → Autotrophic Respiration (R_a)

Soil Moisture, Soil Temperature, Snow Cover → Heterotrophic Respiration (R_h)

Coupling Photosynthesis and Transpiration

PHOTOSYNTHETIC RATE
Gross Primary Production

GPP = PAR x Fpar x ε

Light Use Efficiency
mol C/ mol photon

Evapotranspiration
ET = Transpiration + Evaporation

$$T \sim [e^* - e_a] \frac{g_c g_a}{g_c + g_a}$$

$$g_c = a + b\ GPP \times (h/c)$$

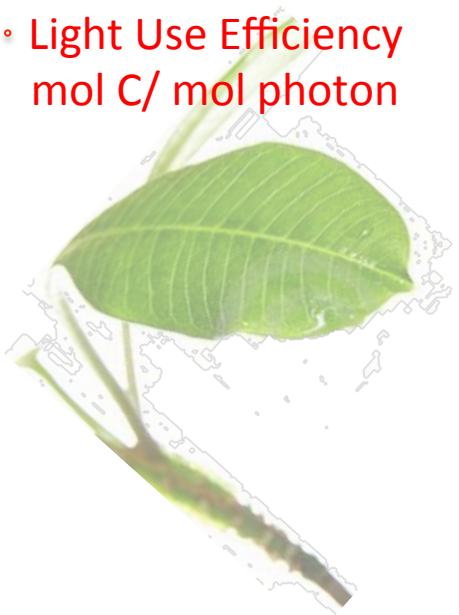

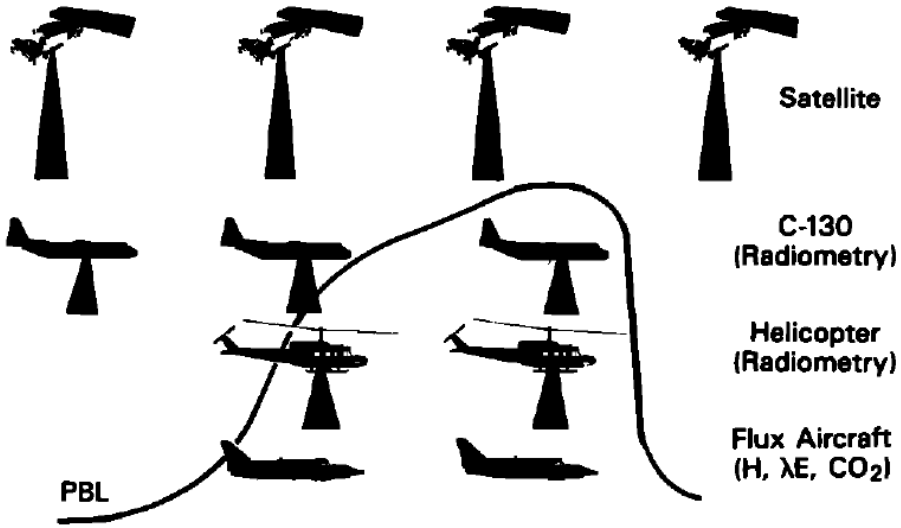

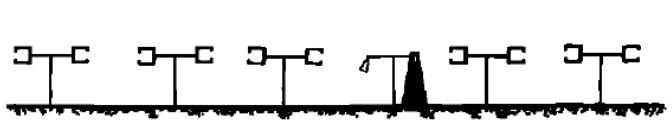

- Simultaneous Radiometric, Energy/Mass Balance Observations at and Above Surface Over Diurnal Cycle
- Coordination With Satellite Overpass

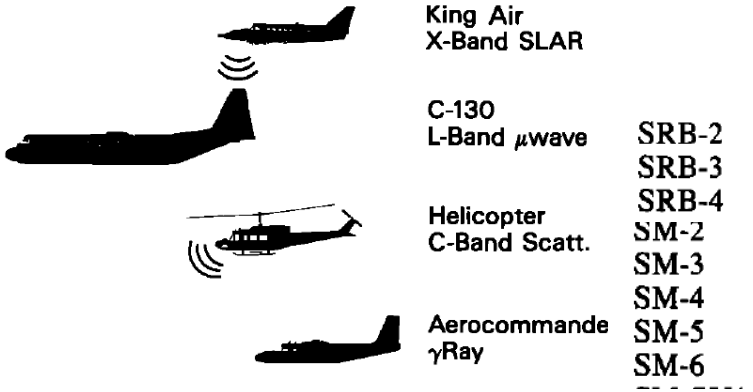

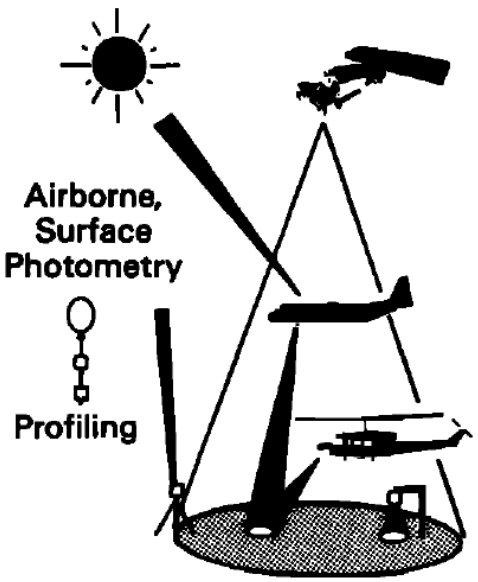

NOAA-9	(1 km)
C-130	(10 m)
Helicopter	(10 m)
Surface	(1 m)

- Simultaneous Radiometric Observations From All Altitudes, All Resolutions
- Coordinated Photometry and Radiosonde Profiling for Atmospheric Corrections

Blad	Surface radiometer
Deering	Surface radiometer (PARABOLA, SE-590)
Irons	Airborne pointable scanner (ASAS)
Peck	NOAA airborne γ ray sensor
Ungar	Impedance probe
Van Zyl	NASA airborne SAR
Wang	NASA C-130 radiometer (PBMR)
Moore/Gogenini	Airborne, helicopter radar/scatterometer

JOURNAL OF GEOPHYSICAL RESEARCH, VOL. 97, NO. D17, PAGES 19,061–19,089, NOVEMBER 30, 1992

Satellite Remote Sensing of Surface Energy Balance: Success, Failures, and Unresolved Issues in FIFE

FORREST G. HALL, KARL F. HUEMMRICH, SCOTT J. GOETZ, PIERS J. SELLERS, AND JAIME E. NICKESON

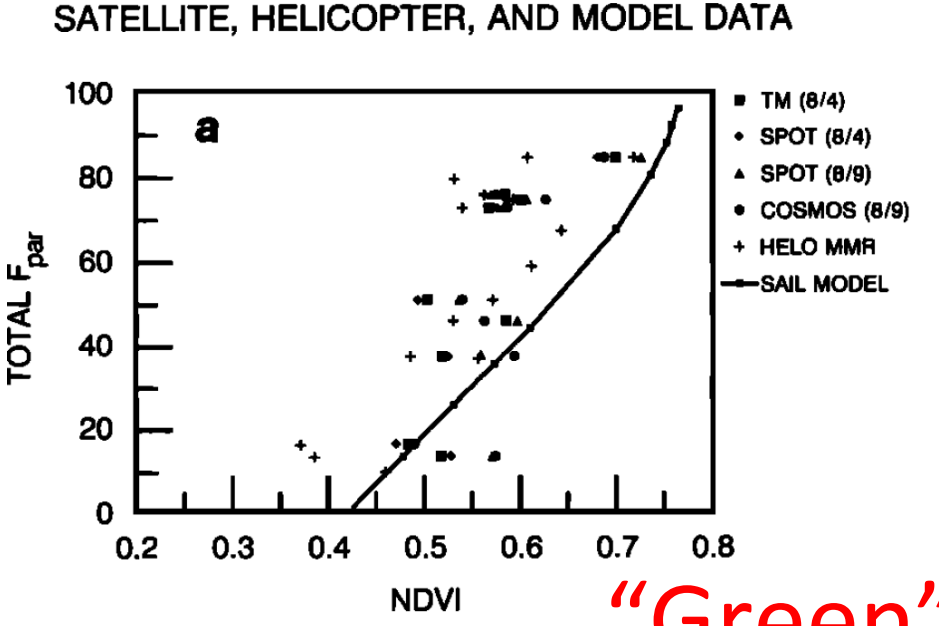

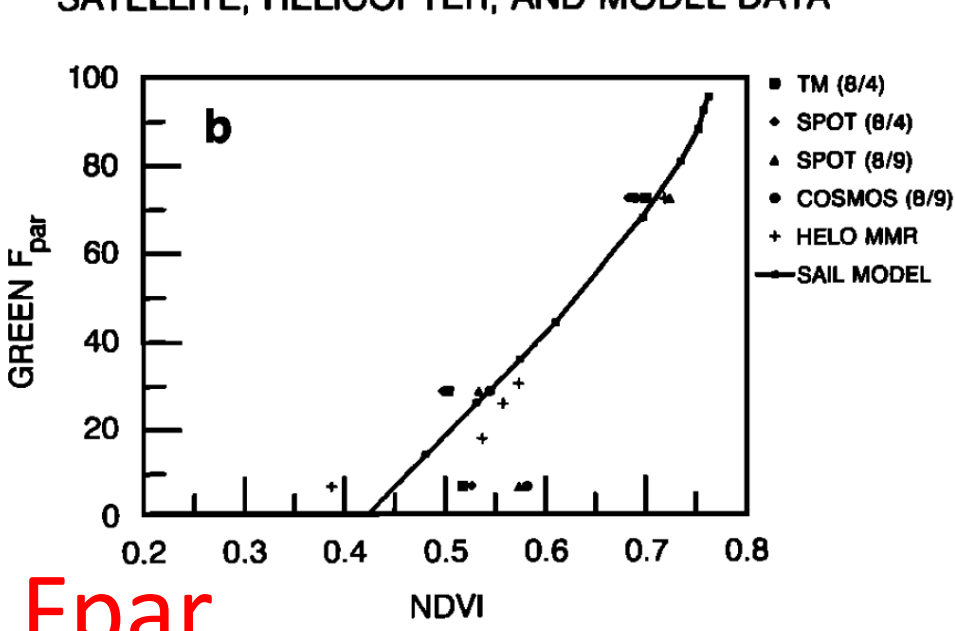

"Green" Fpar

LE

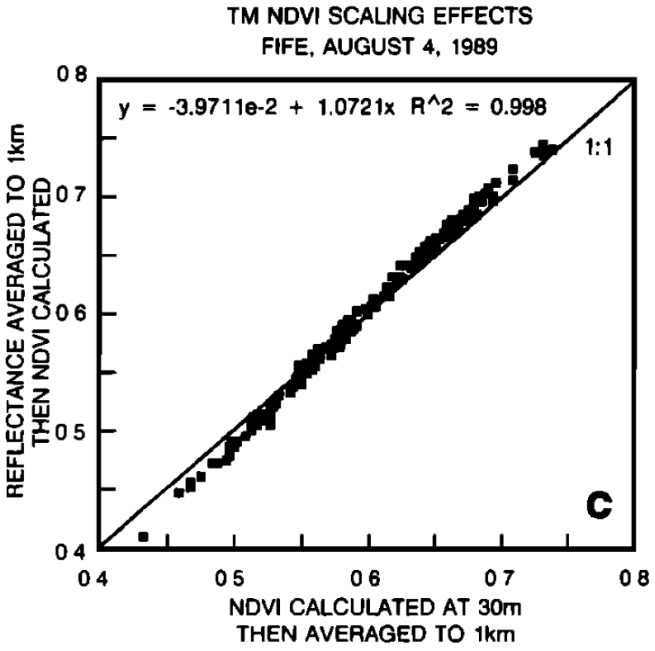

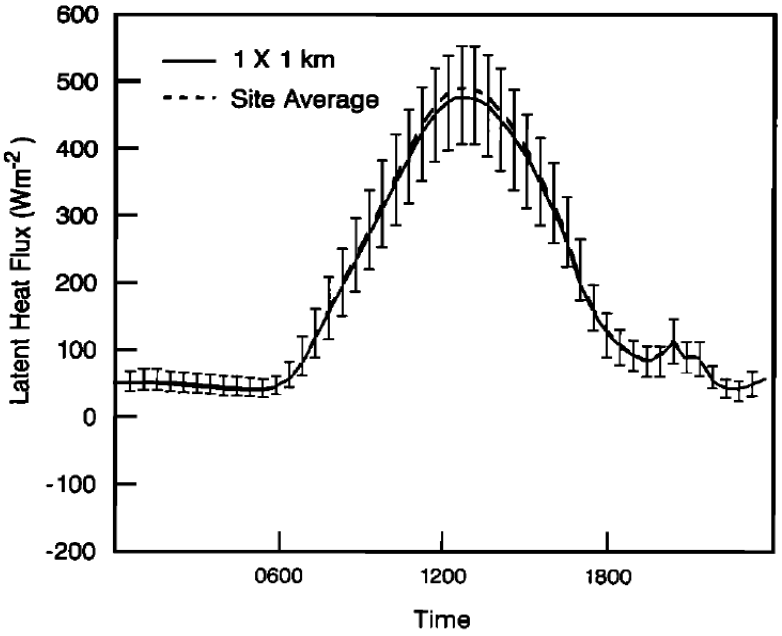

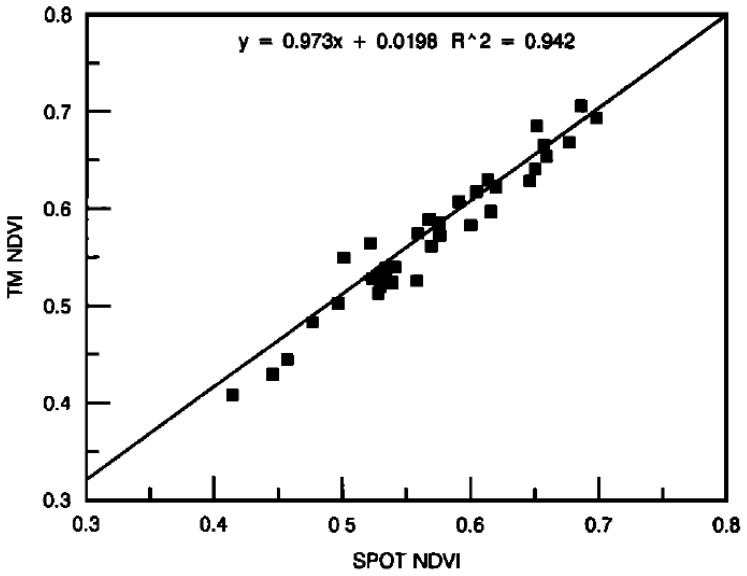

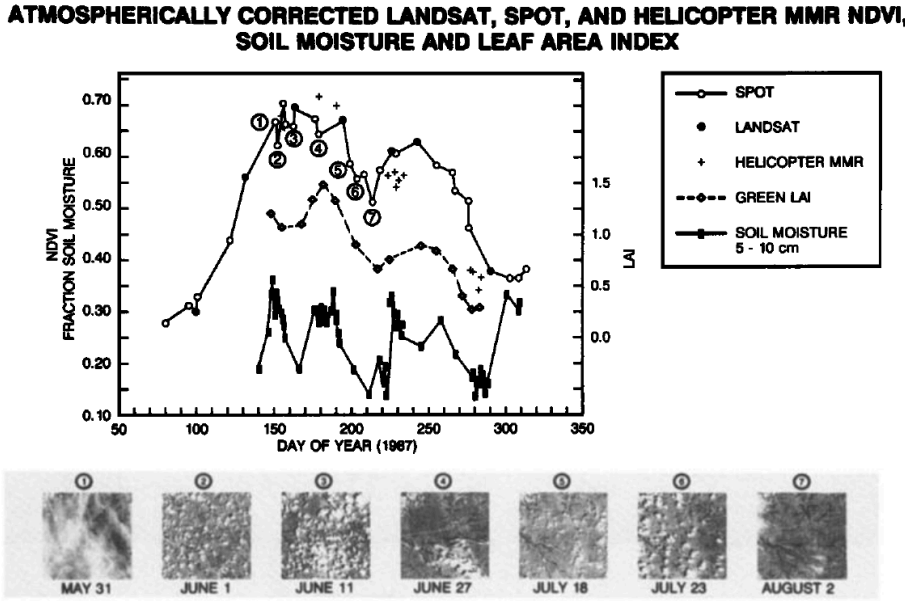

Correction and Calibration

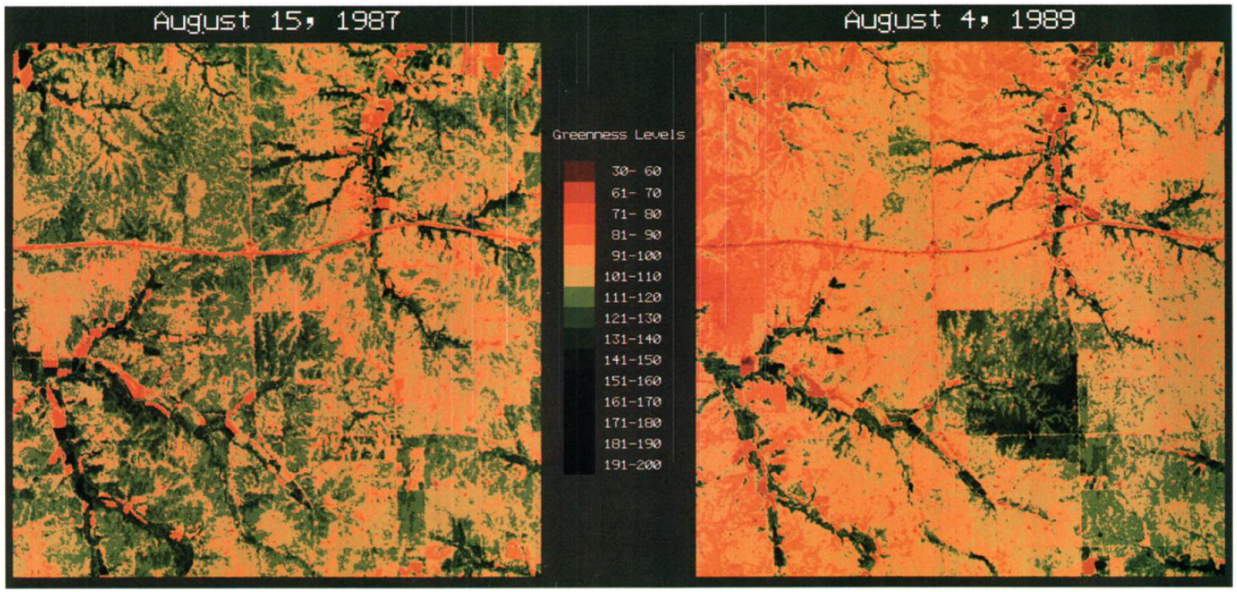

Plate 1. Radiometrically rectified TM images for August 15, 1987, and August 4, 1989. The images are color-coded, transformed Kauth-Thomas greenness values.

Sensible Heat

$$H = \frac{\rho c_p \left(T_c - T_A\right)}{r_a}$$

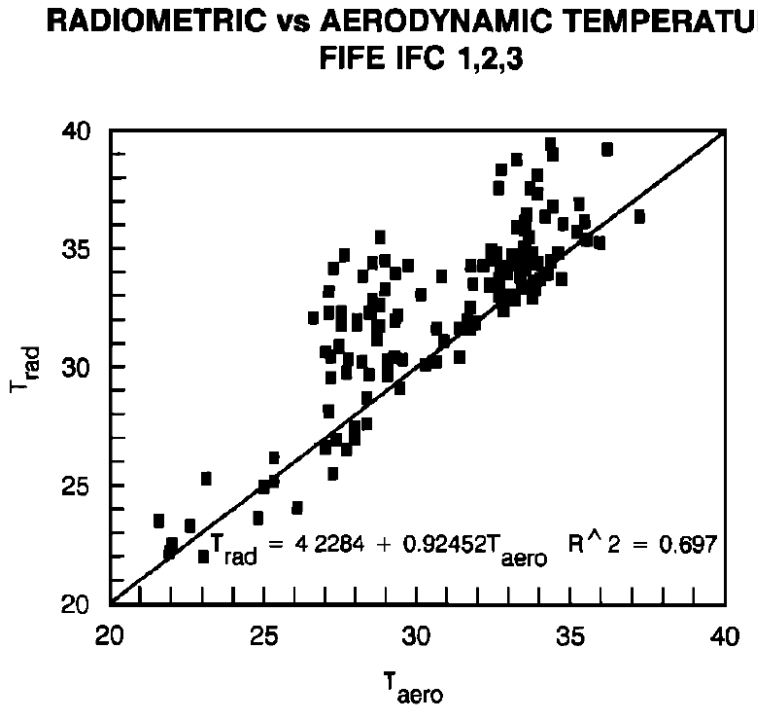

Fig. 8. Radiometric temperature from the nadir-viewing, helicopter-mounted MMR acquired for June 6, July 11, and August 15, 16, and 17, 1987, versus aerodynamic temperature, as calculated from flux station measurements and (3) and (4).

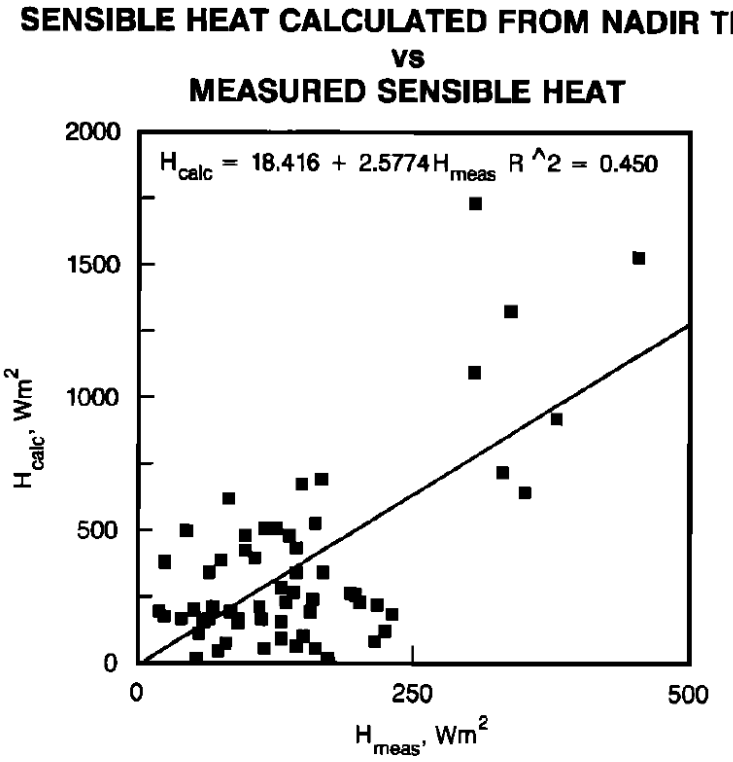

Fig. 9. Sensible heat calculated using radiometric temperature from the nadir-viewing, helicopter-mounted MMR acquired for June 6, July 11, and August 15, 16, and 17, 1987, versus measured sensible heat.

SCALE INVARIANCE

Are the averaged aggregated values the same as the average value?

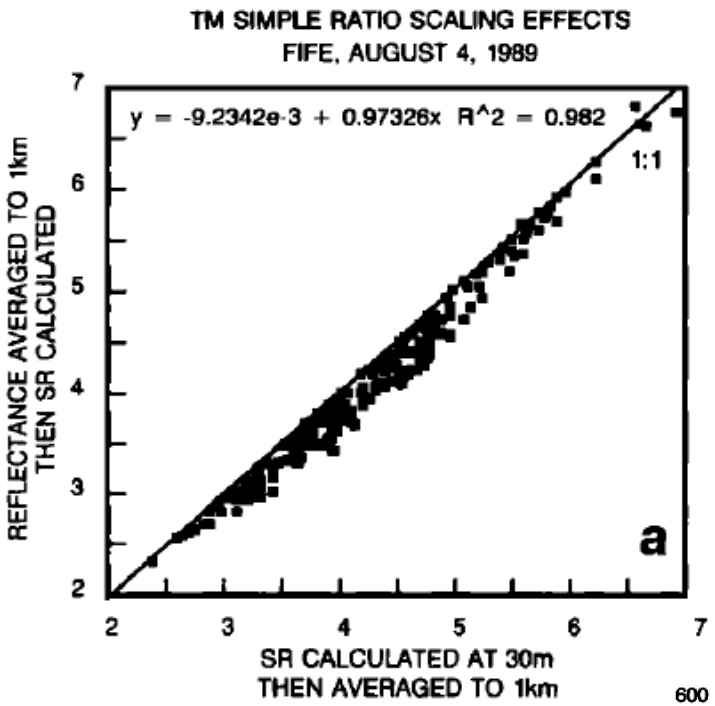

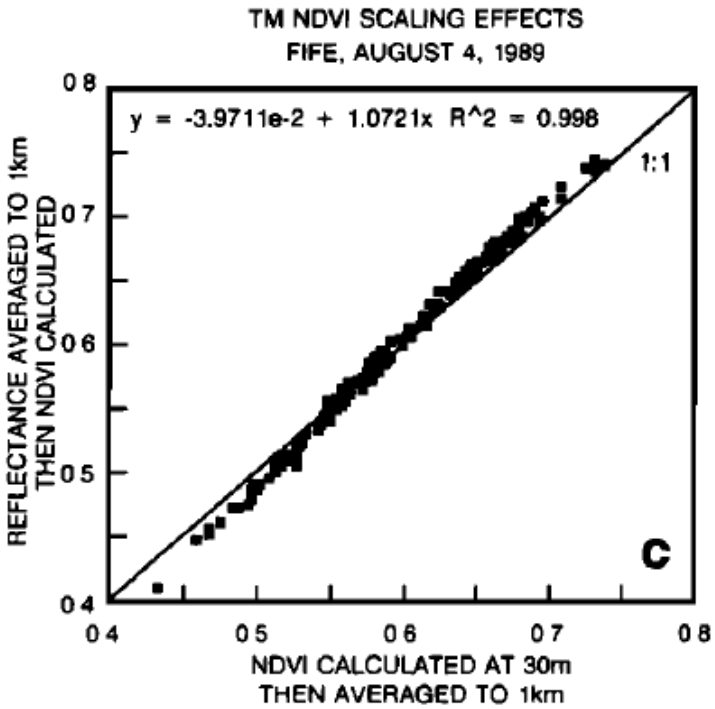

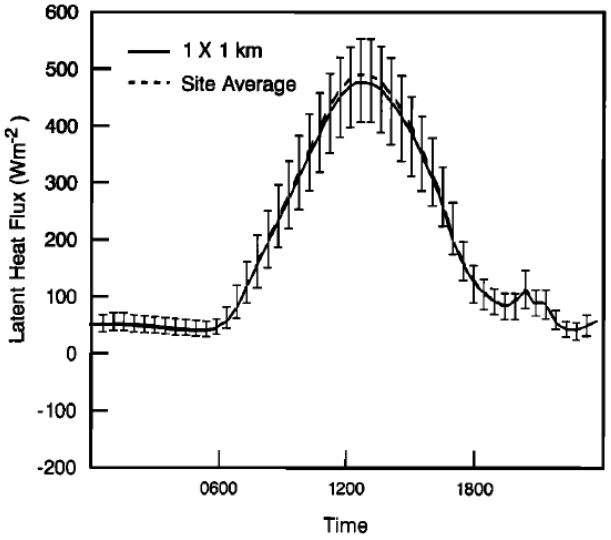

REMOTE SENSING IN FIFE

- Developed remote sensing algorithms to produce seasonal, annual and decadal maps of vegetation type and biophysical properties at regional and global scales.
- Developed a quantitative methodolgy for using vegetation indices to monitor surface energy, water and carbon exchange.
- Developed a physical understanding of what vegetation indices were measuring and their dependence on extraneous effects such as atmospheric and sun angle variations.

BOREAS

Remote sensing in BOREAS: Lessons learned

J.A. Gamon[a], K.F. Huemmrich[b,*], D.R. Peddle[c], J. Chen[d], D. Fuentes[a], F.G. Hall[b], J.S. Kimball[e], S. Goetz[f], J. Gu[g], K.C. McDonald[h], J.R. Miller[i], M. Moghaddam[h], A.F. Rahman[j], J.-L. Roujean[k], E.A. Smith[l], C.L. Walthall[m], P. Zarco-Tejada[n], B. Hu[i], R. Fernandes[o], J. Cihlar[o]

- MAJOR CONTRIBUTION TO NASA'S 21ST CENTURY DECADAL SURVEY RECOMMENDED MISSIONS
  - Radar
  - Passive microwave
  - Lidar
  - Optical
- MULTI-PLATFORM, MULTI-ALTITUDE CAPABILITY DEMONSTRATED SCALABILITY TO SPACE FOR KEY VEGETATION, SOIL AND CLIMATE MEASUREMENT ALGORITHMS

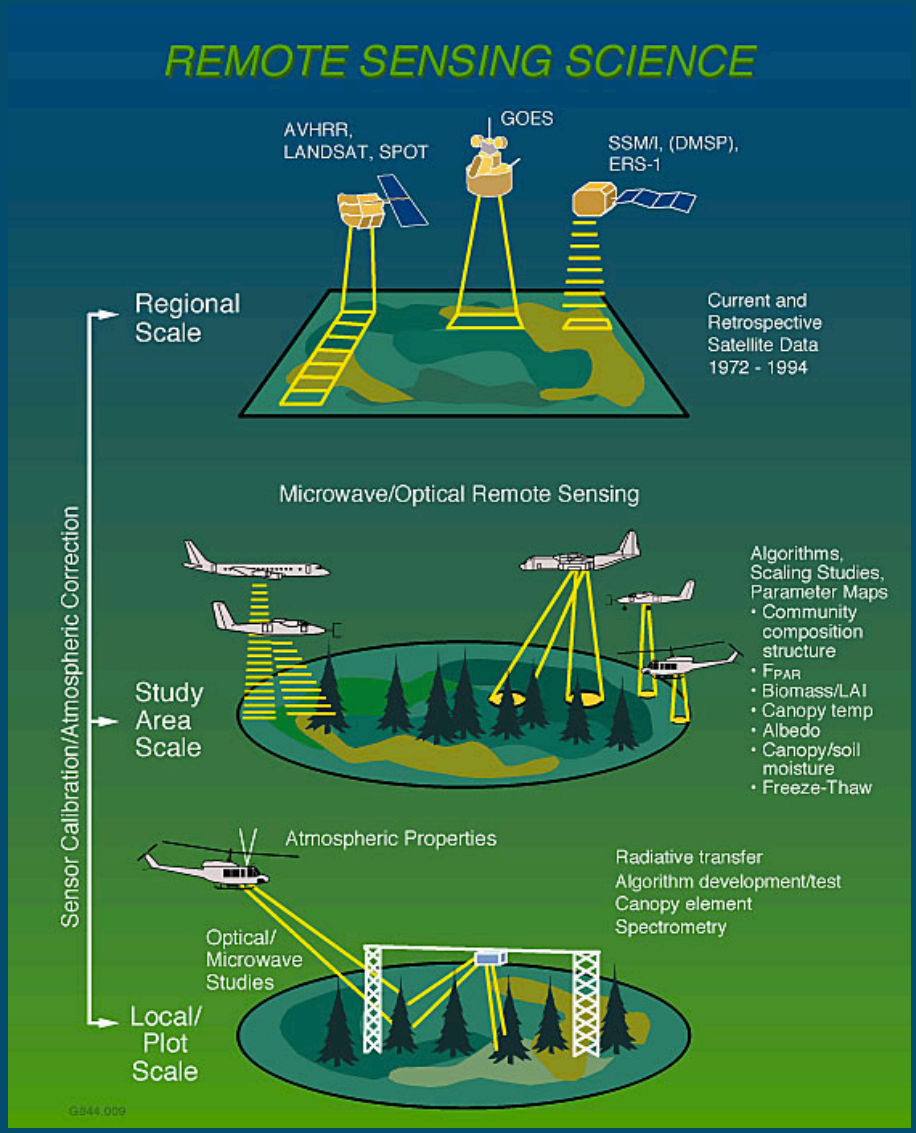

Radar Freeze/Thaw

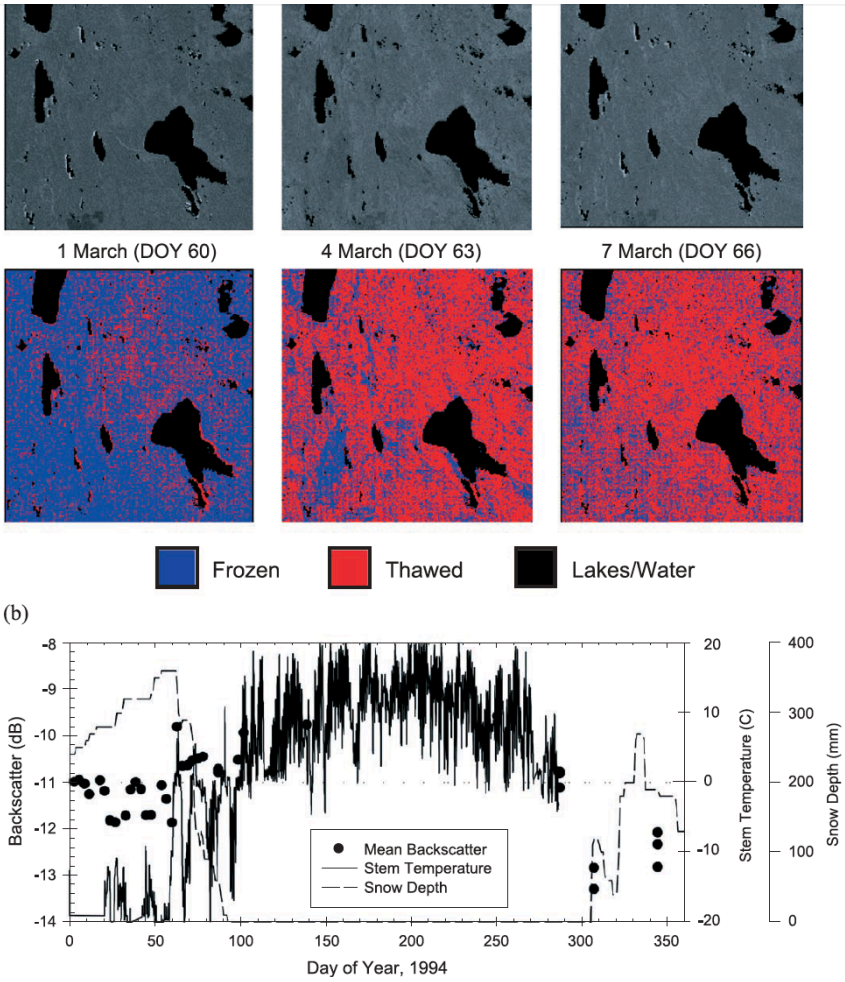

Radar backscatter revealed a relatively simple method for characterizing spring thaw and fall freeze.

Frolking et al., Kimball et al., Goulden et al., Myneni et al.

Fig. 6. (a) Sequence of ERS Synthetic Aperture Radar backscatter images (top row) and corresponding classifications (second row) for three dates in 1994 (day of year also indicated) in the BOREAS SSA, illustrating the radar's ability to monitor thaw processes related to the start of growing season and initiation of photosynthetic processes in the vegetation. (b) ERS-1 SAR backscatter from the SSA Old Black Spruce site compared with tree stem temperature and snow depth.

Carbon/Water Coupling

$$LE = \frac{\rho C_p}{\gamma}[e^* - e_a]\ g_c g_a$$

$$g_c = GPP \times (h/c)$$

GPP = PAR x Fpar x ε

CO_2

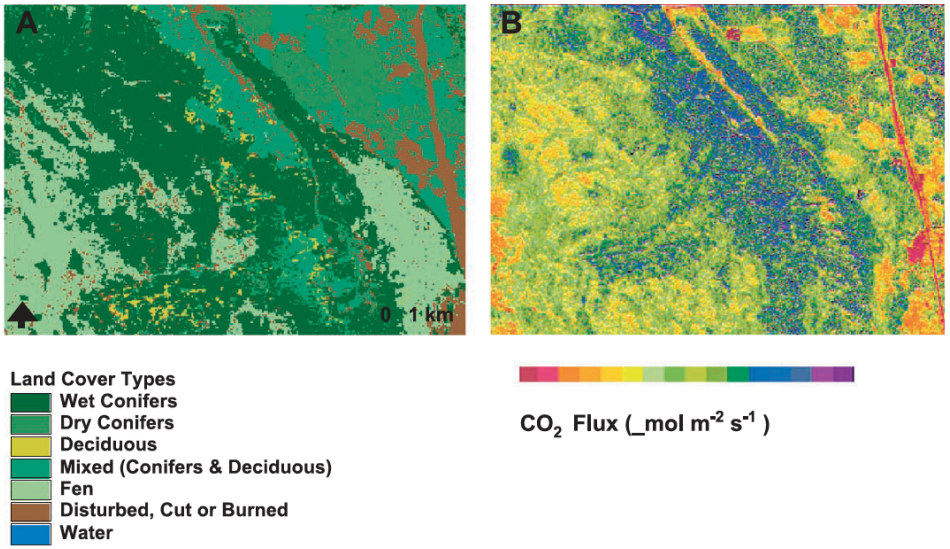

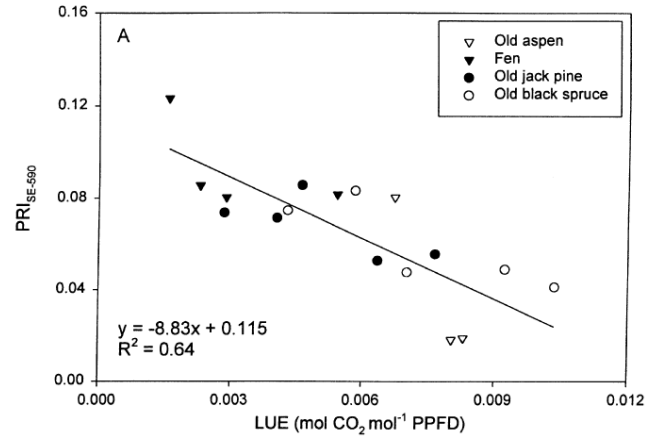

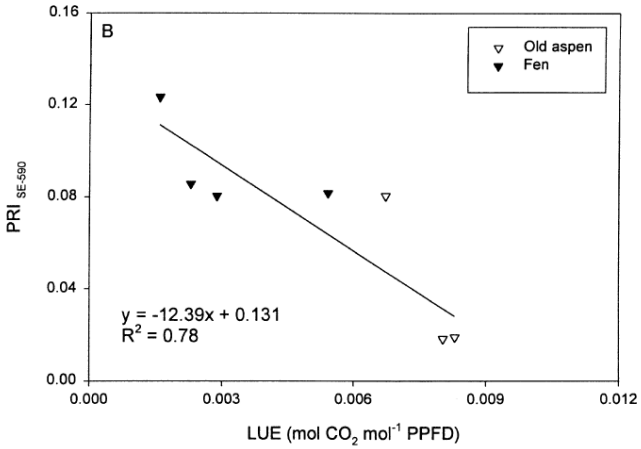

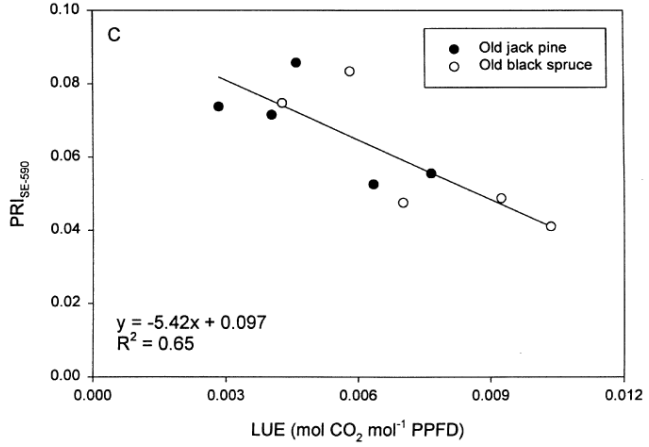

Fig. 4. Comparison of land-cover types (A) with midday gross carbon uptake rates (2-h averages near solar noon) derived from AVIRIS imagery fo of the SSA. The land-cover types were derived from pigment and water absorption features using a combination of spectral mixture analysis and a likelihood classification (Fuentes et al., 2001). The CO_2 flux image (B) was derived from NDVI and scaled PRI using a light-use efficiency model an an empirically calibrated regional image of midday fluxes for September 16, 1994. This method yielded a strong agreement ($r^2 = 0.8$) with fluxes dete eddy covariance from five different boreal ecosystems (Rahman et al., 2001).

Remote sensing of ε across sites

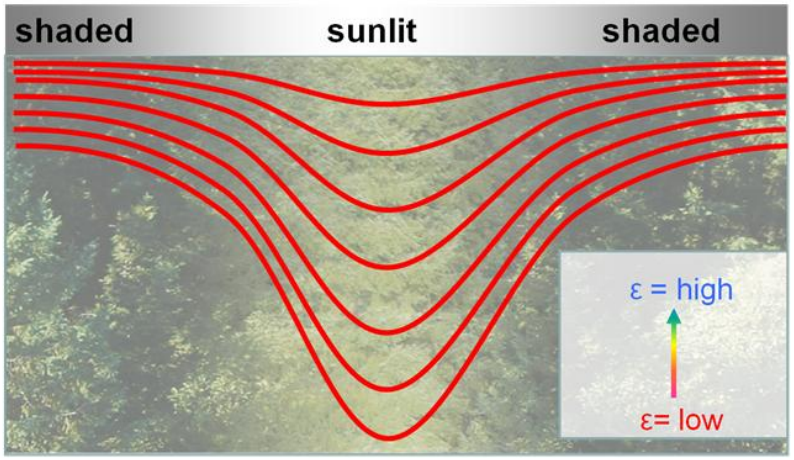

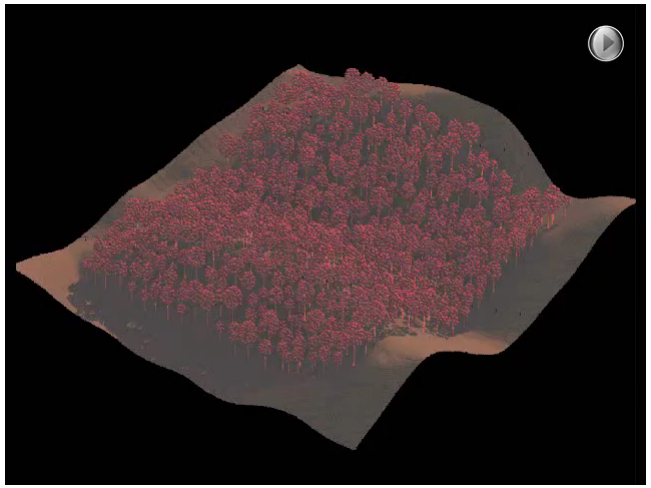

Amspec vs Tower

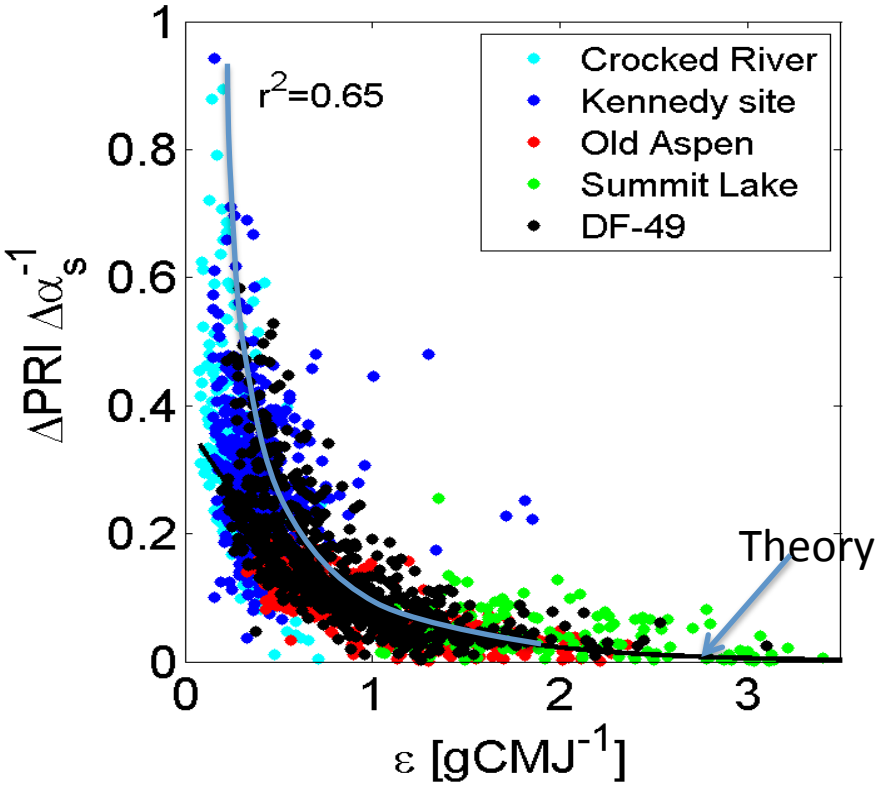

CHRIS/PROBA vs Tower

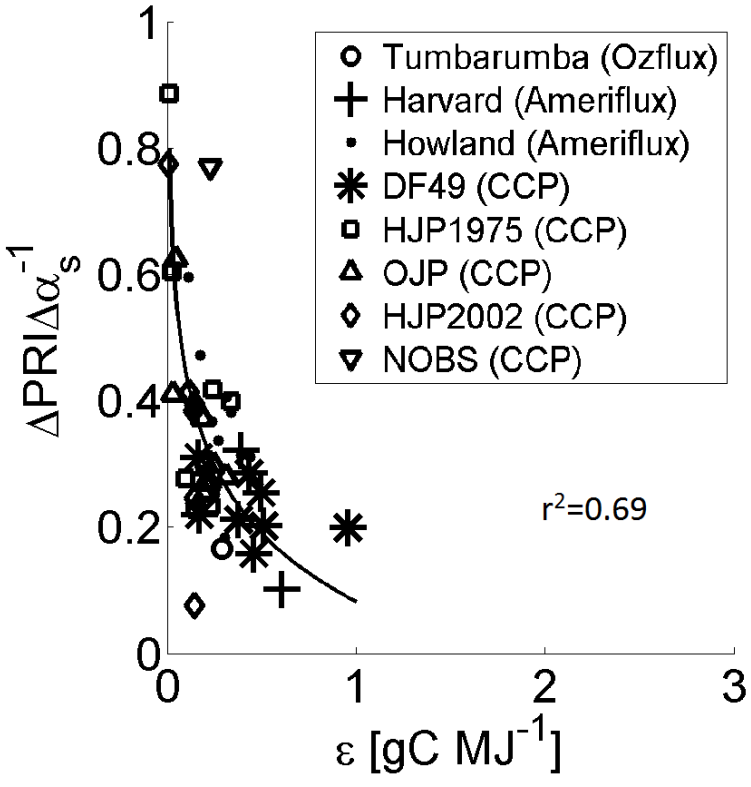

Satellite scale experiment

1 Mature Doug Fir
2 Mature Deciduous
3 Med Age Jack Pine
4 Mature Aspen
5 Young Jack Pine
6 Mature Deciduous
7 Mature Black Spruce
8 Eucalyptus
9 Mature Jack Pine

Temporal Scaling of Photosynthesis

Data assimilation

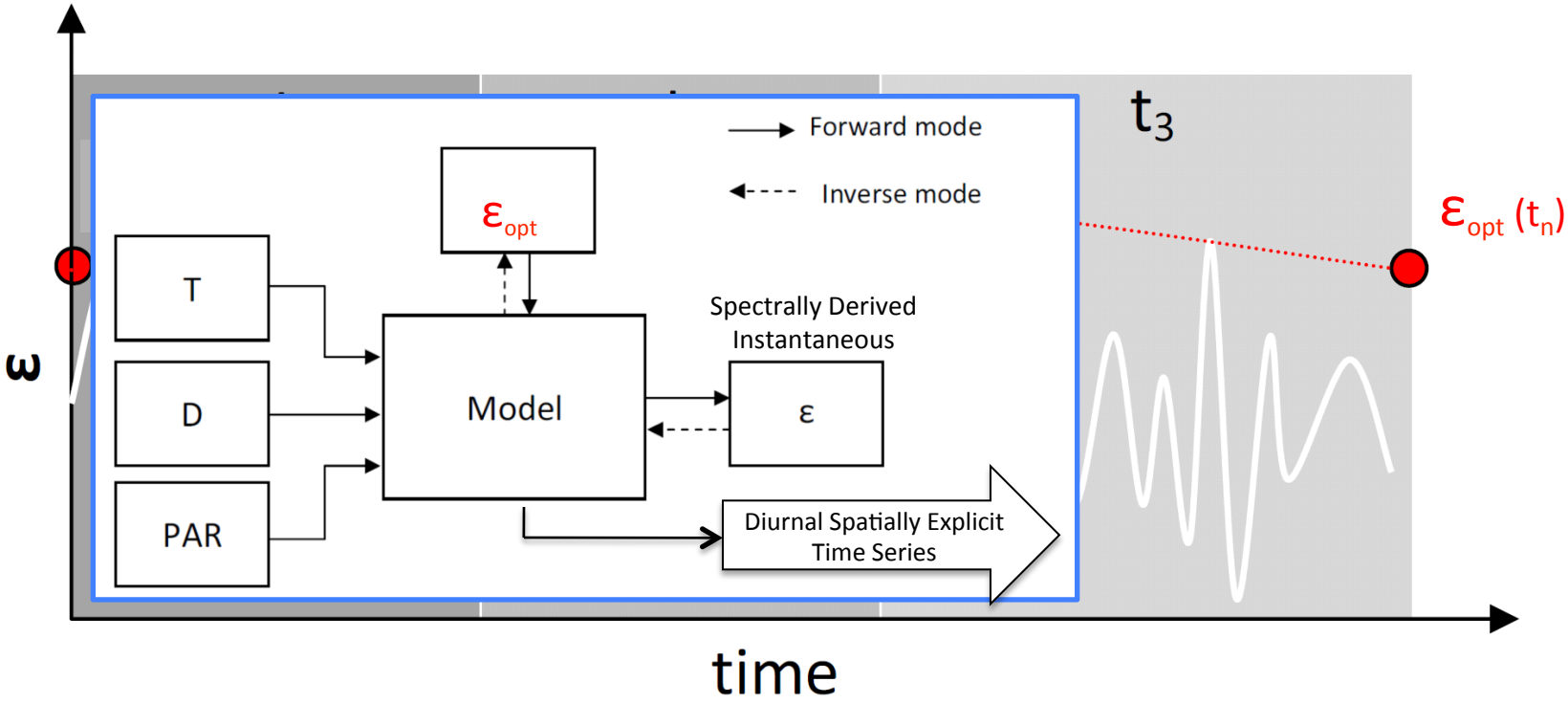

Hilker et al., Remote Sensing of Environment (submitted)

BIOMASS

- Polarimetric radar data from AIRSAR were used to estimate biomass of the southern study area (Saatchi and Moghaddam, 2000)
- SLICER – Scanning Lidar Imager of Caropies by Echo Recovery) flown on aircraft demonstrated the potential for lidar estimates of biomass density (Lefsky et al., 2002)

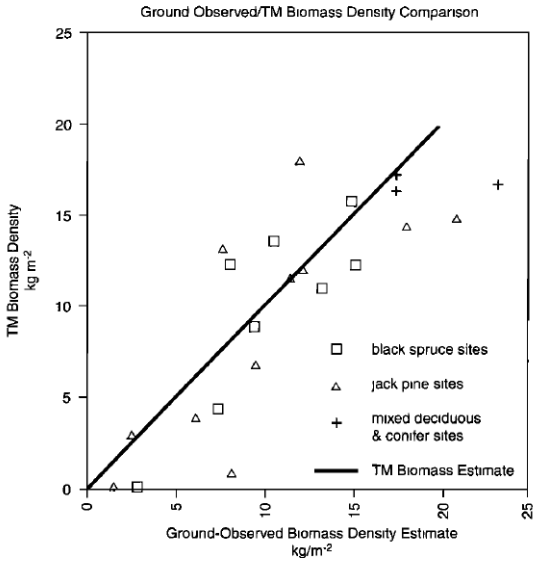

RMS Error Biomass Density 4 kgm^{-2}

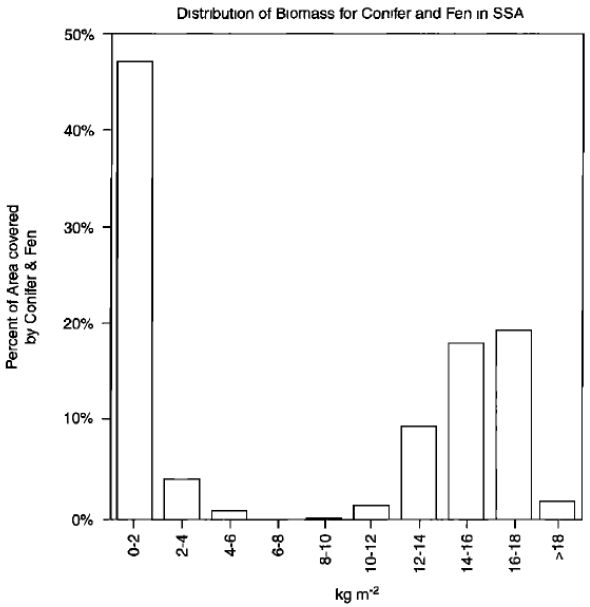

Figure 6. Bimodal distribution of BMD values over the BOREAS SSA. The 0–6 km^{-2} values correspond to sparsely treed fens on peat, whereas the 10–18 kg m^{-2} values correspond primarily to black spruce growing on shallow to deep mineral soils.

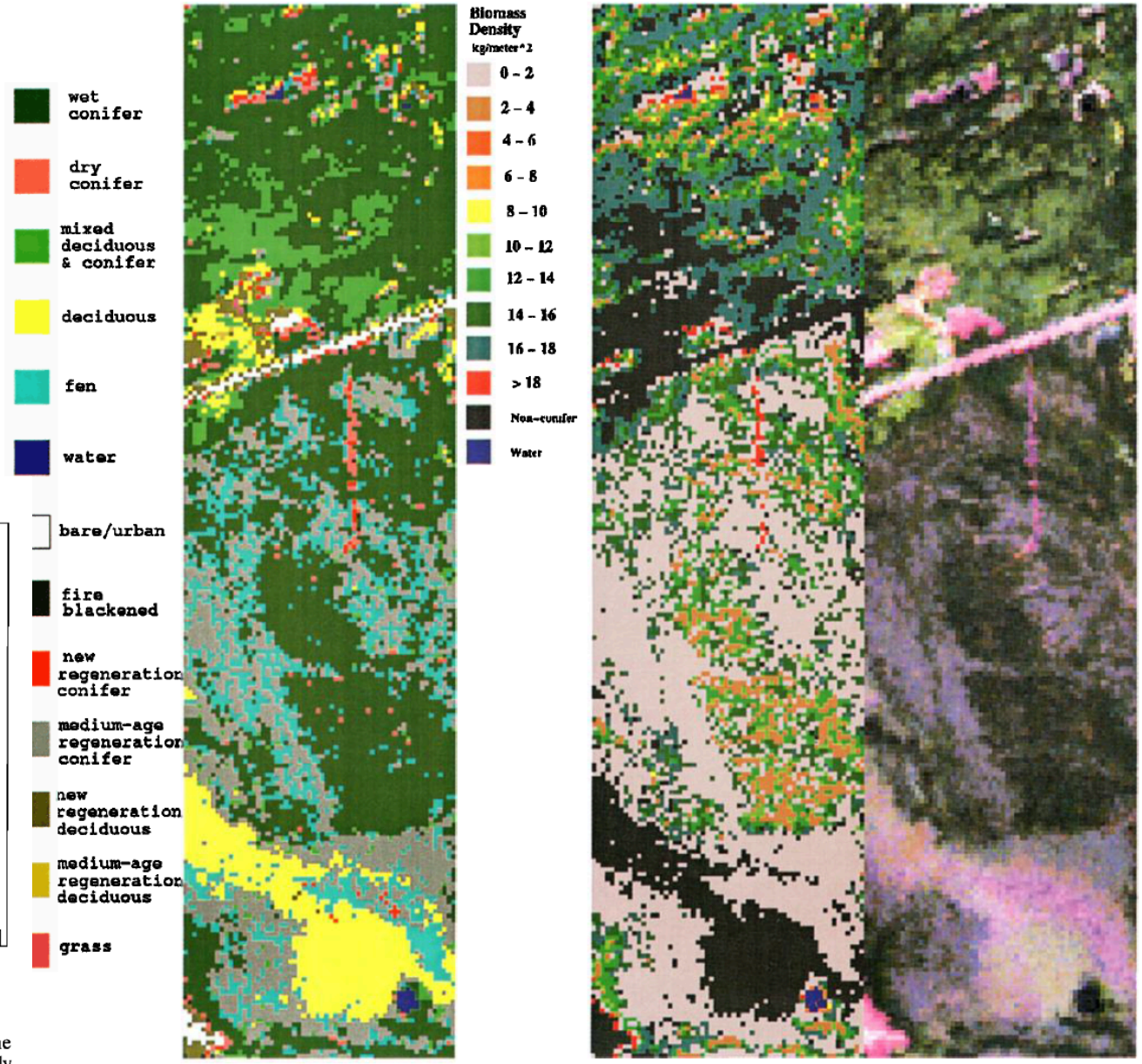

Plate 3. (a) Classification image, (b) BMD image, (c) color MIR image of an ~2 × 7 km area in the BOREAS SSA, including the old black spruce tower site.

Table 2
Summary of BOREAS land-cover classification products published in BOREAS Special Issues and BOREAS data reports

Reference [BOREAS Team]	Sensor	Algorithm	Classes	Area	Image date(s)	Number Classes	Accuracy % (Kappa)	Validation source	Comments
Hall & Knapp, 1994 [TE-18]	Landsat-5 TM (30 m) Bands 1–5,7	maximum likelihood	TE/RSS classes	SSA:NSA: 10^4 km^2 each	August 6, 1990; August 20, 1988	11 (8 forest); 11 (8 forest)	67% (0.56); 73% (0.63) [five classes each]	<27 sites 37 sites, n=333 TF/Aux Sites, 3 × 3 pixels/site	initial product
Hall & Knapp, 1999a [TE-18]	Landsat-5 TM (30 m) Bands 1–5,7	maximum likelihood	TE/RSS classes	SSA: 10^4 km^2	August 6, 1990	11 (8 forest)	78% (0.66) [five classes]	27 sites, n=243 TF/Aux Sites, 3 × 3 pixels/site	updated validation of initial product
Hall & Knapp, 1996; Hall et al., 1997 [TE-18]	Landsat-5 TM (30 m) Bands 3,4,5 reflectance	physically based canopy modeling	TE/RSS classes	SSA: 10^4 km^2	September 2, 1994	13 (9 forest)	70% (0.59) [nine classes]	35 sites, n=315 TF/aux sites, field 3 × 3 pixels/site	includes biophysical parameters; initial product
Hall & Knapp, 1999b [TE-18]	Landsat-5 TM (30 m) Bands 3,4,5 reflectance	physically based canopy modeling	TE/RSS classes	SSA:NSA: 10^4 km^2 each	September 2, 1994; June 21, 1995	13 (9 forest); 11 (8 forest)	75% (0.70); 85% (0.83)	48 sites, n=432, 68 sites, n=612 TF/aux sites, field sites 3 × 3 pixels/site	update SSA new NSA includes biophysical parameters
Peddle, 1999; Peddle et al., 1997 [TE-18, RSS-19]	Landsat-5 TM (30 m) Bands 3,4 reflectance	GOMS physical canopy model and evidential reasoning	TE/RSS classes	SSA	September 2, 1994	13 (9 forest)	85% (0.83)	40 sites, n=992, TF/aux sites, field sites 5 × 5 pixels/site	also has biophysical parameters
Steyaert et al., 1997 [AFM-12, TE-18]	NOAA-11 AVHRR NDVI composites (1 km)	unsup. clustering; field labels	TE/RSS classes	region 5 × 10^5 km^2	April–September 1992	16 (9 forest)	class areas: (relative comparison—no %, K)	agreement with Hall and Knapp (1994) TM products (SSA, NSA)	also mapped forest fires
Cihlar et al., 1997 [TE-16]	NOAA-11 AVHRR composites (1 km)	ECM and CPG	IGBP	full region 10^6 km^2	April–October 1993	32; grouped to 5 (4 forest)	57% (0.30) [all] to 89% (0.78) [pure pixels only]	agreement with Hall and Knapp (1994) TM products (SSA, NSA)	Canada-wide land cover, biophysical products
Ranson et al., 1997 [RSS-15]	SIR-C/XSAR & Landsat TM	maximum likelihood and PCA	forest species/ nonforest	SSA (~MSA) 3 × 10^3 km^2	1994—Radar: April 15/October 6; TM: September 2	7 (3 forest)	87.3%	62 field plots	also has biophysical information (separate)
Beaubien et al., 1999, 2000 [TE-16]	7 scene mosaic Landsat-5 TM Bands 3,4,5	ECM	IGBP/GOFC	SSA, NSA, transect 10^5 km^2	June–August 1991–1998	28 (17 forest)	91% (0.89)	TF/aux sites, field sites n=238	
Peddle et al. (2003)	7 scene mosaic Landsat-5; Bands 3,4	MFM-5-Scale canopy model	IGBP/GOFC	SSA, NSA, and transect	June–August. 1991–1998	13 forest: 25 classes (17 forest)	85% (0.83); 80% (0.78)	136 field sites; agreement with Beaubien et al., 2000 (n=11,442)	also has biophysical parameters
Zarco-Tejada & Miller, 1999 [RSS-19]	CASI 16 bands 3-m reflectance	red-edge	subset of TE/RSS classes	SSA (~ MSA) 192 km^2	August 1, 1996	7 (4 forest)	61% (0.52)	agreement with SERM map (MSA) n=2646	foliar chemistry parameters possible
Fuentes et al., 2001	AVIRIS 20 m 53 bands (of 224 bands) used	spectral mixture analysis & maximum likelihood	subset of TE/RSS classes	SSA (~ MSA) 120 km^2	April 19, 1994, July 21, 1994, and September 16, 1994	7 (4 forest)	80% (0.77)	agreement with SERM map (MSA) n=700	water and foliar chemistry parameters possible

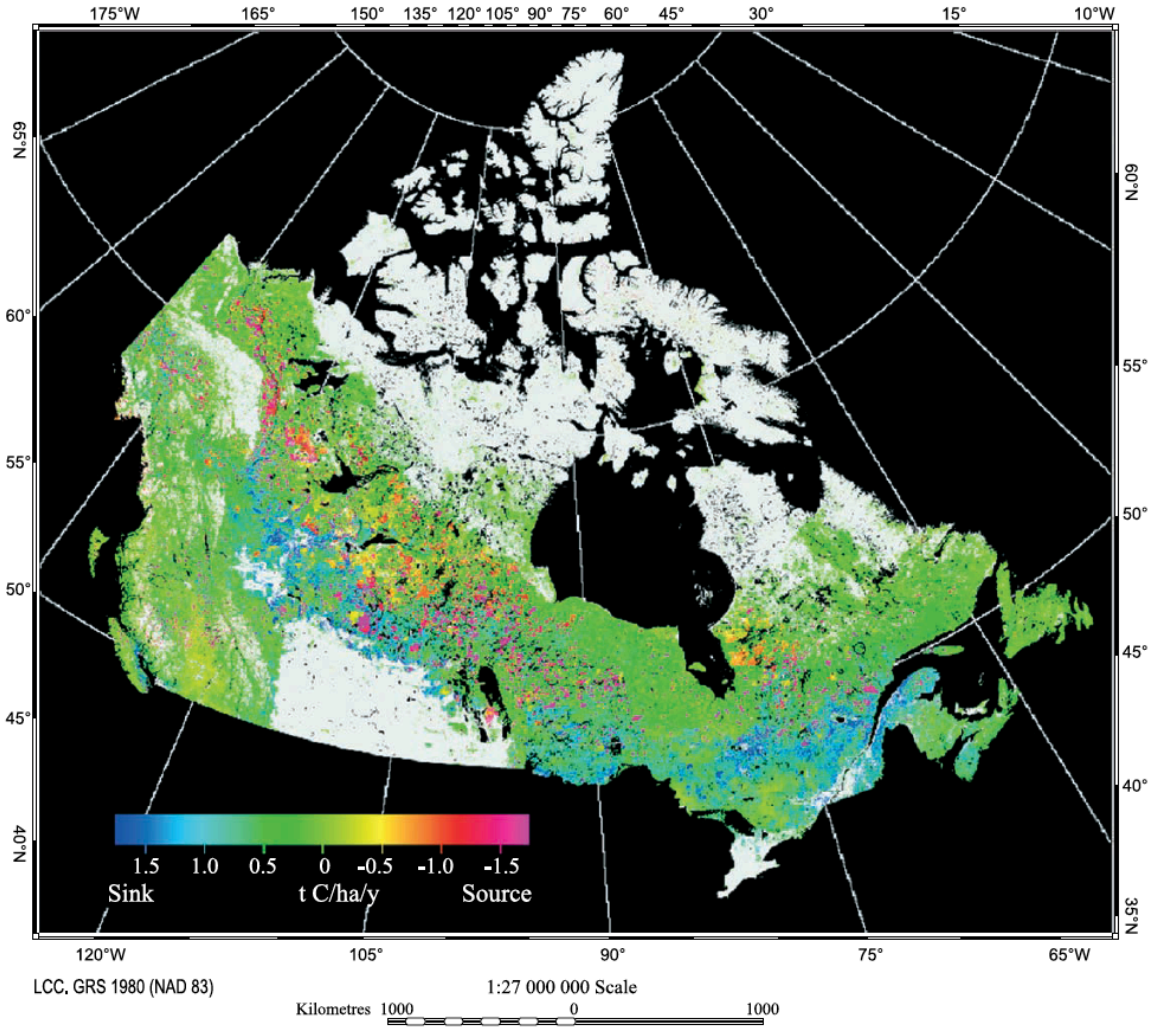

The BOREAS region was found to be a source of carbon during the 1990's because of the increase in fire disturbance, but Canada's forests overall acted as a small sink of about 0.35 $TgCyr^{-1}$ in the same period Chen et al. (2003) .

Number of Publications

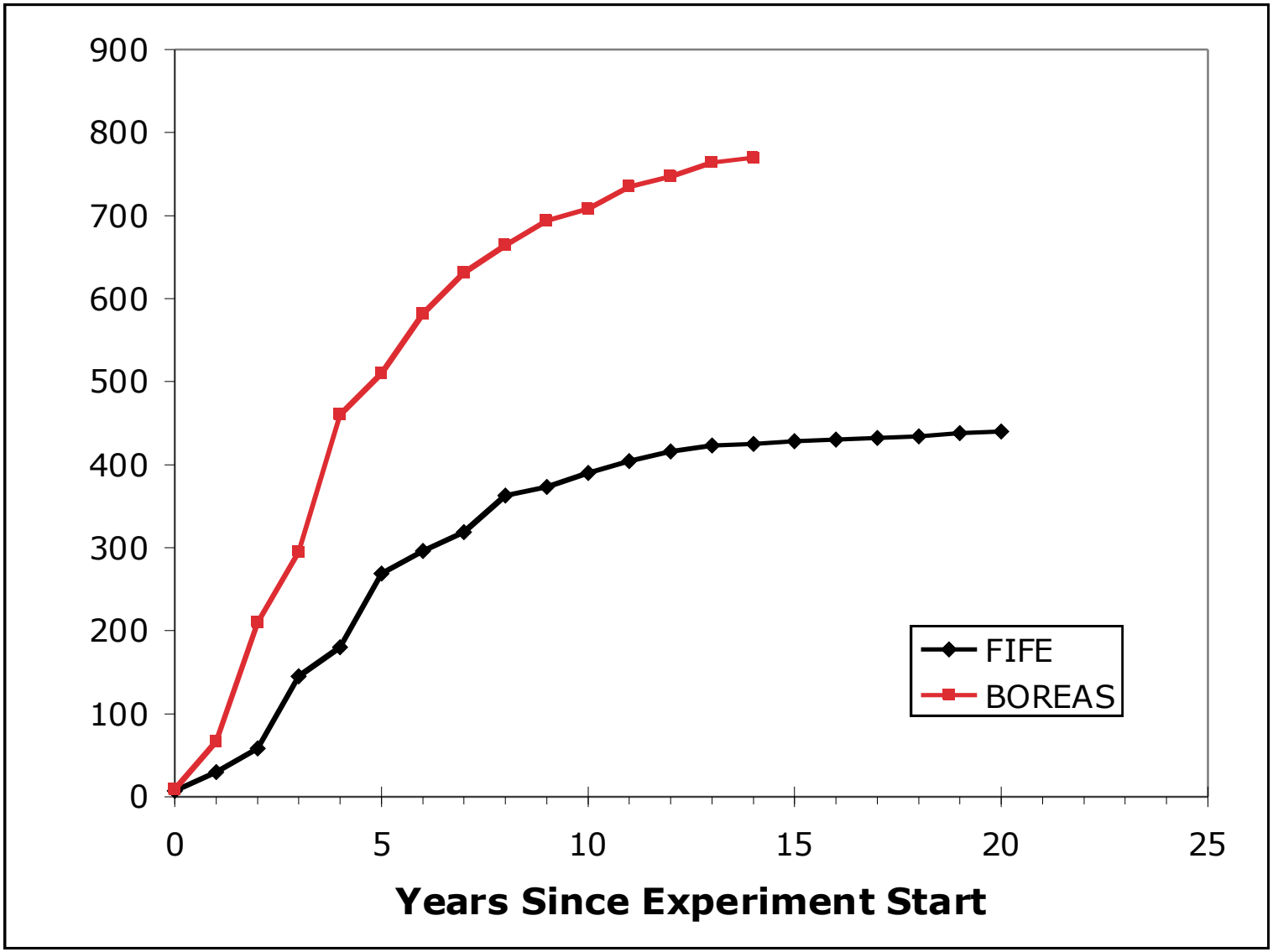

CARBON CYCLE

PROVIDED FOUNDATION FOR EOS DATA PRODUCT ALGORITHMS AND DECADAL SURVEY MISSION CONCEPTS

- HELICOPTER – SPECTROMETER, SCATTEROMETER
- C-130 LIDAR AND MODIS SIMULATOR MEASUREMENTS.
- DC8 MULTIFREQUENCY RADAR
- ER2 AVIRIS HYPERSPECTRAL
- PIPER CHIEFTAN CASI HYPERSPECTRAL

MODIS: 3D VEGETATION PROPERTIES CAN BE INFERRED USING MULTI-ANGLE PASSIVE OPTICAL SENSORS.

GEDI: 3D VEGETATION STRUCTURE AND BIOMASS CAN BE INFERRED USING LIDAR, RADAR AND PASSIVE OPTICAL REMOTE SENSING,

HYSPERI: HYPERSPECTRAL IMAGERS CAN MAP VEGETATION, PHOTOSYNTHETIC AND NON-PHOTOSYNTHETIC STRUCTURE

ENERGY AND WATER CYCLE

- DEMONSTRATION THAT SOIL MOISTURE AND SOIL FREEZE/THAW DATA CAN BE MAPPED REMOTELY
  - DC8 QUAD-POL MULTIFREQUENCY RADAR
  - CV-580 QUAD-POL- MULTIFREQUENCY RADAR
- FIRST DEMONSTRATION THAT VEGETATION PHOTOSYNTHESIS CAN BE MEASURED REMOTELY AND SCALE TO SPACE
  - Helicopter Spectrometer
  - NASA ER2 AVIRIS
- VALIDATION OF ENERGY AND WATER CYCLE MODELS

IMPROVED WEATHER MODELS

- VAST IMPROVEMENTS IN CURRENT WEATHER MODELS AND THEIR GLOBAL FORECASTS.

LEGACY OF FIFE and BOREAS

- Solid Foundation for followon field experiments
  - BERMS, Canadian carbon program
  - LBA
  - ABoVE
- Solid underpinnings for EOS
  - Mission Design
  - Remote Sensing Algorithms
  - Fifteen year time series of key veg states and rates
- Advanced our understanding of the roles played by vegetated surfaces
  - global carbon dynamics
  - Interannual variations in climate, weather patterns
  - How to characterize the ecosystem state and carbon, water and energy cycling rates using modeling and remote sensing.
- Future Remote Sensing Capabilities
  - Lidar
  - Radar
  - Multiangle
  - Hyperspectral
  - Atmospheric CO2 and Methane